Applied Catalysis B: Environmental 127 (2012) 281–290

Contents lists available at SciVerse ScienceDirect

Applied Catalysis B: Environmental

journal homepage: www.elsevier.com/locate/apcatb

Catalytic upgrading of biomass pyrolysis vapors using transition metal-modified ZSM-5 zeolite

E.F. Iliopoulou[a,*], S.D. Stefanidis[a,b], K.G. Kalogiannis[a], A. Delimitis[a], A.A. Lappas[a], K.S. Triantafyllidis[c]

[a] Chemical Process Engineering Research Institute, CERTH, P.O. Box 60361, Thermi, 570 01 Thessaloniki, Greece
[b] Department of Mechanical Engineering, University of Western Macedonia, 50100 Kozani, Greece
[c] Department of Chemistry, Aristotle University of Thessaloniki, 54124 Thessaloniki, Greece

ARTICLE INFO

Article history:
Received 27 April 2012
Received in revised form 4 August 2012
Accepted 28 August 2012
Available online 3 September 2012

Keywords:
Lignocellulosic wood biomass
Catalytic biomass flash pyrolysis
Bio-oil
Zeolites
Transition metals
Nickel
Cobalt

ABSTRACT

The main objective of the present work was the study of different ZSM-5 catalytic formulations for the *in situ* upgrading of biomass pyrolysis vapors. An equilibrium, commercial diluted ZSM-5 catalyst was used as the base case, in comparison with a series of nickel (Ni) and cobalt (Co) modified variants at varying metal loading (1–10 wt.%). The product yields and the composition of the produced bio-oil were significantly affected by the use of all ZSM-5 catalytic materials, compared to the non-catalytic flash pyrolysis, producing less bio-oil but of better quality. Incorporation of transition metals (Ni or Co) in the commercial equilibrium/diluted ZSM-5 catalyst had an additional effect on the performance of the parent ZSM-5 catalyst, with respect to product yields and bio-oil composition, with the NiO modified catalysts being more reactive towards decreasing the organic phase and increasing the gaseous products, compared to the Co_3O_4 supported catalysts. However, all the metal-modified catalysts exhibited limited reactivity towards water production, while simultaneously enhancing the production of aromatics and phenols. An interesting observation was the in situ reduction of the supported metal oxides during the pyrolysis reaction that eventually led to the formation of metallic Ni and Co species on the catalysts after reaction, which was verified by detailed XRD and HRTEM analysis of the used catalysts. The Co_3O_4 supported ZSM-5 catalysts exhibited also a promising performance in lowering the oxygen content of the organic phase of bio-oil.

1. Introduction

An approximate 50% increase above 2002 level is expected in world energy demand, which is nowadays mainly fulfilled from the conventional energy resources like coal, petroleum oil and natural gas. Global energy crisis, including depleting deposits and consequent increasing prices of petroleum oil, combined with environmental problems and concerns, strongly motivated our society to search for alternative, renewable energy sources and specifically liquid transportation fuels [1–3]. Currently, biomass is the fourth largest source of energy in the world after coal, petroleum oil and natural gas, and provides about 14% of the world's energy consumption [4], while it is the most abundant renewable source of carbon, which can be converted to solid, liquid and gaseous fuels, as well as chemicals through various conversion processes [5]. Biomass conversion is conducted via two generic approaches: (thermo)chemical decomposition including gasification, bio-carbonization, liquefaction and thermal decomposition (pyrolysis) processes and biological digestion essentially referring to microbial digestion and fermentation [6,7].

Among the thermochemical conversion processes, biomass flash pyrolysis (BFP) seems to be the most emerging technology for the production of liquid oil (bio-oil), which is considered to be a very promising biofuel/bioenergy carrier, as it can be easily transported, burned directly in thermal power stations or in gas turbines and utilized into a conventional petroleum refinery for the production of higher quality light hydrocarbon fuels. However, bio-oil usually presents several disadvantageous characteristics, such as high water and oxygen content, corrosiveness, instability under storage and heating conditions, immiscibility with petroleum fuels, high acidity, high viscosity, and low calorific value; all these become the primary obstacles for its direct application as a fuel [8,9]. Catalytic pyrolysis of biomass has been introduced in order to improve the quality of the bio-oil. The specific function of various catalysts can alter the product yields and selectivity, thus affecting the composition of the bio-oil and its physical and chemical properties. Several types of microporous (e.g. zeolites: Y, ZSM-5, Mordenite and Beta) and mesoporous (e.g. MCM-41, MSU, SBA-15) materials have been studied as catalysts for biomass pyrolysis or for the upgrading of bio-oil [8–16].

* Corresponding author. Tel.: +30 2310 498312; fax: +30 2310 498380.
E-mail address: eh@cperi.certh.gr (E.F. Iliopoulou).

0926-3373/$ – see front matter © 2012 Elsevier B.V. All rights reserved.
http://dx.doi.org/10.1016/j.apcatb.2012.08.030

Zeolite catalysts are very acidic, ZSM-5 being also very shape-selective due to its small/medium pore size, coupled with its two-dimensional channel-like pore system. In petroleum oil cracking/pyrolysis, H-ZSM-5 induces various reactions, such as protolytic cracking or β-scission, alkylation, isomerization, cyclization, oligomerization and aromatization. The same reactions can take place in the biomass pyrolysis process; however prior to these hydrocarbon-based reactions, the deoxygenation of the holocellulose and lignin fragments of biomass occurs via dehydration and decarbonylation/decarboxylation reactions [9,10,17]. Among zeolites, ZSM-5 has been mainly investigated as a catalyst for biomass pyrolysis and found to dramatically change the composition of the bio-oils by both reducing the amounts of oxygenated compounds via deoxygenation reactions and simultaneously increasing the aromatic species, producing an organic fraction (bio-oil) that can be upgraded to gasoline and diesel type fuels [9–12,18–21]. In addition, the molecular weight of the bio-oil is decreased. The use of ZSM-5 catalyst is reported to reduce oxygen content in bio-oil from 33 to 13%. Oxygen removal was found to take place as H_2O at lower temperatures and as CO and CO_2 at higher temperatures [22,23]. The latter case is preferable, as more hydrogen would be accessible for hydrocarbon formation and consequently less carbon would deposit on the zeolite, while at the same time the water content of bio-oil is reduced [12]. Oxygen removal, primarily in the form of water, results from the H-ZSM-5 stronger dehydration tendency due to its strong acidity [24]. However, the strong acidity of ZSM-5 leads to the decrease of the organic fraction of bio-oil via overcracking towards hydrocarbons, gases or coke formation. The acid sites are therefore the essential part of the mechanism for both the deoxygenating reactions and the deactivating mechanisms [10]. Overall, tuning of the acid sites availability is important in designing the catalyst, as it affects the selectivity of the system, but also the extent of coke formation. Many acid sites give a high yield of gasoline-like products, but this also leads to high affinity for coke formation [25].

The presence of transition metals is suggested to affect the mode of oxygen rejection by producing more carbon oxides and less water, making that way more hydrogen available for incorporation into hydrocarbons. Thus, transition metal modified zeolite catalysts (CeZSM-5, CoZSM-5, CoHZSM-5, H[AlFe]ZSM-5, GaZSM-5, HZSM-5, and NiZSM-5) were used in biomass pyrolysis as an attempt to verify if these metal promoted zeolitic materials of reduced acidity can produce higher yields of hydrocarbons and less coke than commercial ZSM-5 catalysts tested before [26–30]. Indeed the highest yield of hydrocarbons (approximately 16 wt.%, including 3.5 wt.% of toluene) was achieved using nickel, cobalt, iron and gallium-substituted ZSM-5 [26]. Introduction of 1 wt.% Ga into HZSM-5 was also tested for bio-oil upgrading purposes and was found to increase the bio-oil yield as well as the selectivity to aromatic hydrocarbons [27,28]. The incorporation of a transition metal (nickel) in the HZSM-5 zeolite was considered to increase the yield of aromatics and the hydrothermal stability of the catalyst, a behavior attributed to the dehydrogenating activity of nickel and to the fact that the doped catalyst has moderate acid strength [29]. Metal modified mesoporous Al-MCM-41 have also been studied in the pyrolysis of biomass. Iron and copper modified, as well as the parent MCM-41, were the optimum catalysts for the production of phenols. The most important finding in the gaseous pyrolysis products was the increased concentration of the hydrogen in the presence of transition metals, especially when applying Cu–Al-MCM-41 [31]. Moreover, the catalytic activity of Ni-based catalysts using alumina, ceria and alumina/ceria as supporting materials during pyrolysis of paper biomass sample was recently reported at high temperatures and with varying residence time. According to the gas analysis result, 30 wt.% Ni doped alumina sample produced the maximum amount of H_2 production with 43.5 vol.% at 800 °C (using a 15 min residence time) [32].

On the other hand, industrial scale application of biomass pyrolysis i.e. using the circulating fluid bed (CFB) technology, one of the most promising processes for the continuous biomass catalytic conversion to bio-oil, necessitates catalyst regeneration due to coke formation [33–35]. Adequate stability of the catalyst throughout the continuous reaction-regeneration steps should be considered during the design of the most appropriate catalyst formulations. Thus, it seems that research challenges on biomass catalytic pyrolysis include among others (tailoring of porosity and acidity of the candidate catalytic materials, etc.), resistance to catalyst deactivation and improved catalyst hydrothermal stability and attrition resistance.

In the present study we have investigated a commercial catalytic formulation, as candidate catalyst for biomass pyrolysis, which comprises of about 30 wt.% crystalline ZSM-5 zeolite (the rest being silica–alumina) and has been previously transformed into equilibrium state by subjecting it to successive reaction-regeneration steps in a continuous biomass fast pyrolysis circulating fluid reactor (pilot plant unit). More specifically, we evaluated the promotion of this catalyst with transition metals (Ni and Co), studying the effect of metal type, loading and oxidation state on product yields and composition of the biomass pyrolysis oil. Ni and Co were selected, as these metals are expected to affect the mechanism of oxygen removal, as well as the hydrogen transfer reactions during the catalytic upgrading of biomass pyrolysis vapors.

2. Experimental

2.1. Biomass feedstock

A commercial lignocellulosic biomass (Lignocel HBS 150-500) originating from beech wood was used in the current study (45.98 wt.% carbon, 6.39 wt.% hydrogen, 46.28 wt.% oxygen, 1.35 wt.% ash, 43.8 mg/kg Na, 326 mg/kg K), consisting of 1.35% ash, 3.74% extractives, 21.75% lignin, 33.91% hemicellulose and 39.25% cellulose. For the analysis of biomass composition, prior to any other analysis, biomass was extracted with a mixture of ethanol and toluene at a ratio of 1:2 for 16 h, while the extracted sample was dried in an oven at 105 °C for 24 h. The official method TAPPI222 was then followed for the determination of the lignin content, while the holocellulose content was determined with small modifications of the well-established Wise method. The determination of the cellulose content was based on the official method TAPPI203 and the hemicellulose content of the samples was determined by subtracting the determined α-cellulose content from the holocellulose. Before the pyrolysis experiments the Lignocel feed was dried at 105 °C for 4 h and kept in a desiccator, therefore all results reported in this study are on a dry feed basis. The ash content of biomass was measured with a method similar to the ASTM E1755-01 method and was determined as the solid residue after dry oxidation of biomass in air at 575 °C for 12 h. The moisture was determined by drying at 105 °C for 4 h. C and H content were determined by elemental analysis using a LECO-800 CHN analyzer.

2.2. Preparation and characterization of catalytic materials

The catalytic materials used for the biomass pyrolysis experiments were a crystalline ZSM-5 zeolite (Zeolyst CBV8014, SiO_2/Al_2O_3 molar ratio = 80) and a commercial equilibrium ZSM-5 diluted with silica–alumina (containing 30 wt.% crystalline zeolite); this latter zeolitic catalyst was further promoted with Ni or Co (1, 5 and 10 wt.%) via a typical wet impregnation method using aqueous solutions of $Ni(NO_3)_2{\cdot}6H_2O$ and $Co(NO_3)_2{\cdot}6H_2O$ salts. The

Co-based catalysts were calcined at 500 °C/6 h/air, while the Ni-based catalysts were calcined at 600 °C/5 h/air. For comparison, catalytic pyrolysis experiments with NiO, CoO, Co_3O_4, were also conducted. The same calcination conditions were applied for the preparation of the NiO, Co_3O_4, pure metal oxides starting from the same corresponding nitrate salts, while CoO was a commercial reactant supplied by Sigma–Aldrich.

The various catalytic materials were analyzed by Inductive Coupled Plasma – Atomic Emission Spectroscopy (ICP-AES) for the determination of their chemical composition (wt.% of Al and Na for the zeolites and Ni and Co for the metal-modified catalysts), using a 4300 DV PerkinElmer Optima spectrometer.

X-ray diffraction (XRD) measurements were also performed using a SIEMENS D-500 diffractometer employing $CuK\alpha_1$ radiation ($\lambda = 0.15405$ nm) and operating at 40 kV and 30 mA. The XRD patterns were accumulated in the range of 5–75° 2θ every 0.02° (2θ) with counting time 2 s per step. In the case of the transition metal supported catalysts, the average crystal size of the Ni- or Co-based phases was estimated by applying the Scherrer equation:

$$L = K \times \frac{\lambda}{B \times \cos(\theta)} \quad (1)$$

where L is the average crystal size (approximation), K is a constant (typically ~0.89) and B is the full width at half maximum of a selected peak at 2θ diffraction angle.

For the determination of surface area (BET method), pore volume and mesopore size distribution (BJH method) N_2 adsorption/desorption experiments were conducted at −196 °C, using an Automatic Volumetric Sorption Analyzer (Autosorb-1MP, Quantachrome). The samples were previously outgassed overnight at 350 °C under 5×10^{-9} Torr vacuum.

High resolution transmission electron microscopy (HRTEM) experiments were carried out in a JEOL 2011 electron microscope, operating at 200 kV with a point resolution of 0.23 nm. The instrument was also fitted with an energy-dispersive X-ray spectroscopy (EDS) detector for the elemental analysis of the samples. Qualitative and semi-quantitative analysis of EDS data was accomplished using the INCA microanalysis software package. The samples were prepared by dispersing the catalyst powders in high-purity ethanol using an ultrasonic apparatus. A drop of the sonicated solution was subsequently deposited onto a lacy carbon-film supported on a Cu grid and allowed to evaporate under ambient conditions.

Fourier-Transform Infrared (FT-IR) spectroscopy experiments, combined with in situ adsorption of pyridine for the determination of the Brönsted (band at 1545 cm^{-1} attributed to pyridinium ions) and Lewis (band at 1450 cm^{-1} attributed to pyridine coordinated to Lewis acid sites) type acid sites of the catalysts, were performed on a Nicolet 5700 FTIR spectrometer (resolution 4 cm^{-1}) using the OMNIC software. Data processing was carried out via the GRAMS software and the quantitative determination of acid sites was performed by adopting the molar extinction coefficients proposed by Emeis [36].

2.3. Biomass flash pyrolysis (non-catalytic and catalytic) experiments

The biomass pyrolysis experiments were performed on a bench-scale fixed bed tubular reactor (ID 1.4 cm, height 36 cm), made of stainless steel 316 and heated by a 3-zone furnace. A specially designed piston system was used to introduce the solid biomass feedstock into the reactor. A detailed description of the experimental unit has been previously reported [14,15]. For comparison purposes, additional pyrolysis experiments were realized using an inert solid heat carrier (silica sand). The amount of biomass used in all experiments was 1.5 g and the amount of silica sand (in non-catalytic experiments) or of catalyst (in catalytic experiments) was 0.7 g. In a typical pyrolysis experiment, the solid biomass was inserted from the top of the reactor and was pushed down instantaneously with the aid of a piston in the hot reactor zone (at 500 °C). The produced pyrolysis vapors were driven through the catalyst's bed with the aid of the flowing N_2 (100 cm^3/min) for 15 min, while additional purging with N_2 (50 cm^3/min) was performed for another 10 min. A typical residence time of the vapor phase in the catalyst bed was about 0.03 s (supposing utilization of a Fluid Catalytic Cracking (FCC) fixed catalytic bed; FCC apparent bulk density: 0.733 cm^3/g; FCC void fraction: 0.385; catalyst bed volume: 0.97 cm^3). The above described catalytic pyrolysis experiments can be referred to as *in situ* upgrading of pyrolysis vapors and are of the "ex-bed" type (i.e. there was no mixing of solid biomass with the solid catalyst). In addition, all the experimental parameters (i.e., fast heating of biomass, low residence time, fast cooling of products) resemble those of the biomass fast pyrolysis (BFP) type of experiments.

The liquid products (bio-oil) were collected and quantitatively determined using a pre-weighted glass receiver submerged in a liquid bath (−17 °C). The pyrolytic vapors, upon their condensation in the glass receiver, formed multiple phases; an aqueous phase, a liquid organic phase and viscous organic deposits on the receiver walls. For the collection of a representative bio-oil sample, the bio-oil was first fully homogenized inside the receiver using ethyl lactate as the solvent and was collected as a solution, which was then submitted for analysis. Further details on this procedure developed in our laboratory can be found elsewhere [16]. Three experiments under the same conditions were realized for each catalytic material in order to ensure repeatability and the average values from the three experimental runs were used. The standard deviation was, maximum, 1 wt.% on biomass for solid product yields, 1.5 wt.% on biomass for the organic fraction yields and 1.7 wt.% on organic fraction for the oxygen content of the organic fraction.

The water content of the bio-oil was determined by the Karl-Fischer method (ASTM E203-08). The water/aqueous phases present in the bio-oil were separated from the organic phase using an organic solvent (dichloromethane). The organic phase of the bio-oil was analysed by GC–MS using an Agilent 7890A/5975C gas chromatograph–mass spectrometer (Electron energy 70 eV; Emission 300 V; Helium flow rate: 0.7 cm^3/min; Column: HP-5MS (30 m × 0.25 mm ID × 0.25 μm)). Internal libraries were used for the identification of the compounds found in the bio-oil and their categorization into main functional groups. The gaseous products were collected and measured by the water displacement method. The gaseous products were analyzed in a HP 5890 Series II gas chromatograph, equipped with four columns (Precolumn: OV-101; Columns: Porapak N, Molecular Sieve 5A and Rt-Qplot 30 m × 0.53 mm ID) and two detectors (TCD and FID). The amount of the solid residue left in the reactor consisted mainly of charcoal and coke-on-catalyst formed by thermal and/or catalytic cracking and was determined by direct weighting.

3. Results and discussion

3.1. Physicochemical characteristics of catalytic materials

The most important physicochemical properties of the zeolitic (pure and equilibrium/diluted ZSM-5) and Ni and Co based catalytic materials used in the catalytic upgrading of biomass flash pyrolysis vapors are presented in Tables 1 and 2. Zeolite ZSM-5 comprises a 2-D channel-like pore system with perpendicularly intersecting channels of ~0.55 nm in diameter [37]. The surface area of the sample used in the present study was 450 m^2/g and as it is shown by the micropore volume data; it was highly microporous with

Table 1
Chemical composition, porosity and acidity characteristics of zeolitic catalysts.

Catalysts	Chemical composition (ICP-AES)		Porosity characteristics (N_2 porosimetry)				Acidic properties (Pyr-FTIR measurements)	
	Al content (wt.%)	Na content (wt.%)	Surface area[b] (m^2/g)	Pore size (nm)	Micropore volume[c] (cm^3/g)	Meso/ macropore volume[d] (cm^3/g)	Brönsted acidity (μmol/g)	Lewis acidity (μmol/g)
ZSM-5 (pure) (SiO_2/Al_2O_3: 80)	0.85 ± 0.04	0.014 ± 0.002	450	Microporous	0.133	0.140	133.8	32.7
ZSM-5 (diluted)[a]	14.58 ± 0.72	0.231 ± 0.012	138	~4.0[e]	0.037	0.071	36.5	18.1

[a] Commercial equilibrium ZSM-5 zeolite catalyst diluted with silica–alumina (~30 wt.% zeolite); it has been previously tested in a circulating fluid bed pilot plant reactor in biomass fast pyrolysis, being subjected to continuous reaction (500 °C) and regeneration steps (700 °C).
[b] Multi-point BET method.
[c] From *V–t* plot analysis.
[d] From the difference of total pore volume at $P/P_0 = 0.99$ minus the micropore volume.
[e] Due to the mesoporosity of the silica–alumina matrix, estimated by BJH pore size distribution analysis.

few structural and textural defects that generated the observed limited meso/macroporosity. The H^+-exchanged ZSM-5 possesses mainly Brönsted acid sites (bridging hydroxyls connected to framework aluminum atoms) of high acidic strength, in addition to few Lewis acid sites attributed to positively charged tri-coordinated Si atoms and extra-framework octahedrally coordinated, aluminum oxyhydroxy species, which can be generated during the various calcination processes that the zeolite undergoes (i.e., at 550–600 °C initially to remove the organic template of the as-synthesized zeolite and then for converting the NH_4^+-exchanged form to H^+-form) [38–41]. The presence of Lewis acid sites in the pure H-ZSM-5 zeolite was verified by the results of the Py-FT-IR measurements, which are shown in Table 1. Still however, the number of Brönsted acid sites of the H-ZSM-5 zeolite sample used in this study was markedly higher compared to that of the Lewis sites.

On the other hand, the surface area of the equilibrium/diluted ZSM-5 catalytic formulation was lower (~140 m^2/g, Table 1), originating from the micropores of the crystalline ZSM-5 (~30 wt.%) and the mesopores (~4 nm) of the silica–alumina matrix. Accordingly, the micropore volume of this catalyst was significantly lower compared to that of the pure ZSM-5 zeolite, while its meso/macropore volume was higher due to the matrix. With regard to the acidity of the equilibrium/diluted ZSM-5, the number of Brönsted acid sites were significantly lower compared to those of the pure H-ZSM-5 zeolite (less than one-third, in accordance with the percentage of crystalline ZSM-5 in the diluted formulation and the zeolite framework dealumination during regeneration in the pilot plant unit), while the Brönsted to Lewis acid sites ratio was also much lower (2 from 4 in the pure H-ZSM-5), due to the nature of acid sites in the high-alumina matrix and the presence of the extra-framework Si–Al species of the zeolite.

Impregnation of the commercial equilibrium/diluted ZSM-5 catalyst with transition metals had a moderate effect on the porosity characteristics of the parent material. As shown in Table 2 there is no significant loss of the surface area and micro- and meso/macropore volume in the case of the lower metal loadings (1 and 5 wt.%) for both metals (Ni and Co). However, higher loadings (10 wt.%) of either Ni or Co led to 15% and 28% decrease of the surface area respectively, which can be mainly attributed to the blockage of micropores of the embedded crystalline ZSM-5 zeolite by the metal phases formed [19]. The micropore volume of the catalysts was reduced to a greater extent compared to the meso/macropore volume (Table 2).

On the other hand, the effect of metals on the acidic properties of the equilibrium/diluted ZSM-5 zeolitic catalyst was more pronounced (Table 2), compared to the porosity characteristics. The presence of 1 and 5 wt.% Ni or Co reduced the number of Brönsted acid sites (BAS) by 35–50%, while higher loading (10 wt.%) induced further reduction (45–60%). The significant decrease of the number of Brönsted acid sites suggests that part of the acidic protons in crystalline zeolite ZSM-5, which are responsible for the Brönsted acidity of the catalyst, were ion-exchanged by Co or Ni ions during the dry impregnation procedure. In contrast to the Brönsted acid sites, the number of Lewis acid sites (LAS) was increased by ca. 30–60% with both metals, possibly due to the formation of the corresponding oxides, i.e. NiO and Co_3O_4 (based on XRD results), which could function as Lewis acidic centres. Iron modification of a proton form zeolite was also reported to change the distribution of acid sites.

Table 2
Chemical composition, porosity and acidity characteristics of metal-modified ZSM-5 catalysts.

Catalysts	Chemical composition (ICP-AES)		Porosity characteristics (N_2 porosimetry)				Acidic properties (Pyr-FTIR measurements)		
	Nominal metal loading (wt.%)	Actual metal loading (wt.%)	Surface area[b] (m^2/g)	Pore size[c] (nm)	Micropore volume[d] (cm^3/g)	Meso/ macropore volume[e] (cm^3/g)	Brönsted acidity (μmol/g)	Lewis acidity (μmol/g)	Total acidity (μmol/g)
ZSM-5 [a]	–	–	138	4.0	0.037	0.071	36.5	18.1	54.6
Ni(1%)/ZSM-5	1	1.26 ± 0.06	138	3.9	0.037	0.085	21.9	54.9	76.8
Ni(5%)/ZSM-5	5	5.89 ± 0.29	132	3.5	0.036	0.094	21.9	54.6	76.5
Ni(10%)/ZSM-5	10	11.4 ± 0.55	117	3.3	0.032	0.116	19.2	43.6	62.8
Co(1%)/ZSM-5	1	1.13 ± 0.05	138	3.9	0.037	0.098	25.4	39.8	65.2
Co(5%)/ZSM-5	5	5.51 ± 0.25	131	3.6	0.036	0.082	17.3	45.9	63.2
Co(10%)/ZSM-5	10	11.06 ± 0.5	100	3.5	0.027	0.094	13.0	35.4	48.4

[a] Commercial equilibrium/diluted ZSM-5 zeolite catalyst.
[b] Multi-point BET method.
[c] From BJH analysis.
[d] From *V–t* plot analysis.
[e] From the difference of total pore volume at $P/P_0 = 0.99$ minus the micropore volume.

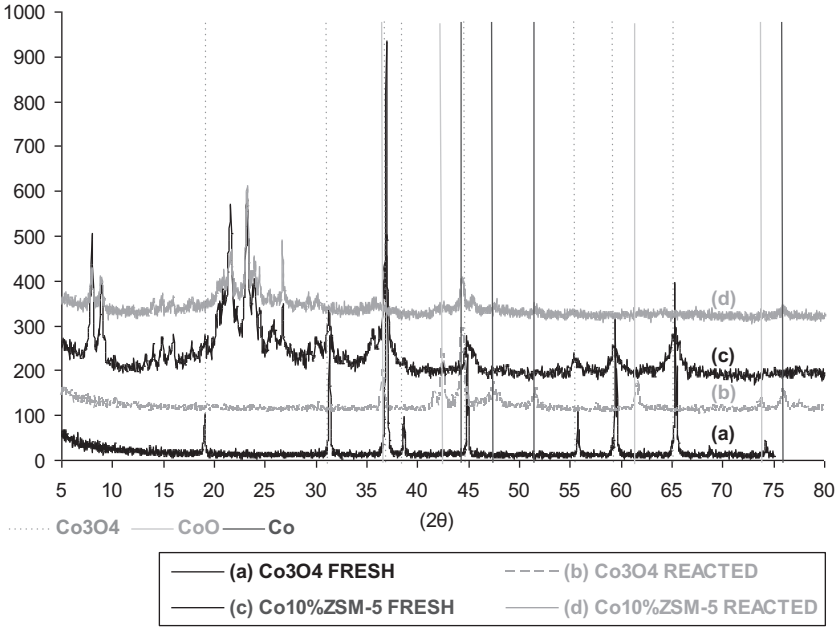

Fig. 1. XRD patterns of fresh/calcined and reacted cobalt catalysts: (a) Co_3O_4 fresh, (b) Co_3O_4 reacted, (c) Co(10%)/ZSM-5 fresh and (d) Co(10%)/ZSM-5 reacted. Identified crystal phases are indicated by dashed and solid lines.

In that case, the strongest acid sites decreased to a higher extent, when the zeolite was modified with iron, while the medium BAS also decreased but not to such extent as the strong ones. Interestingly, the weak LAS were also higher for the iron modified ferrierite and beta zeolites [18].

The XRD patterns of the calcined metal-modified diluted ZSM-5 catalysts and the corresponding pure metal oxide phases are shown in Fig. 1 (as well as in Figures S1 and S2 in Supplementary Information). Almost all the Co-modified ZSM-5 catalysts exhibited XRD patterns with the characteristic peaks of Co_3O_4, whose intensity was increased with Co loading. The size of Co_3O_4 crystals (estimated by the Scherrer equation) increased from 17.9 nm to 22.8 nm for the 5 and 10% Co-loaded catalysts, respectively, while the corresponding peaks in the catalyst with 1 wt.% Co were hardly identifiable. No peaks attributed to CoO species were detected. Fig. 1 shows the XRD patterns of the calcined Co(10%)/ZSM-5 catalyst and Co_3O_4 before and after the biomass pyrolysis tests. Interestingly, either as pure oxide or supported on ZSM-5, Co_3O_4 was reduced to CoO and metallic Co after reaction, due to the reductive atmosphere that occurred during the catalytic pyrolysis of the biomass vapors at 500 °C (more discussion follows below). The size of metallic Co in the used zeolitic catalyst was slightly smaller (19.2 nm, based on Scherrer calculations) compared to that of the corresponding-parent supported Co_3O_4 oxide.

The same observations were noticed for the calcined Ni-loaded ZSM-5 catalysts and the pure NiO, before and after biomass pyrolysis. However, the dispersion of Ni seems to depend more on loading degree as compared to Co, since the crystallite size of NiO increases from 28.5 nm to 39.5 nm for the 5 and 10 wt.% loaded catalysts (the peaks due to NiO in the Ni(1%)ZSM-5 catalyst could be hardly indentified). Furthermore, in this case, the crystallites of metallic Ni after the pyrolysis reaction exhibited much smaller size (18.4 nm) compared to the size of NiO crystals in the catalyst prior to testing.

The size and morphology of the catalysts in the nanoscale was examined by transmission electron microscopy (TEM) experiments that were performed on the metal-modified diluted ZSM-5 catalysts with the highest nominal loading (10 wt.%), both before and after use in biomass pyrolysis tests. A typical bright field (BF) TEM image of the Co(10%)/ZSM-5 catalyst is shown in Fig. 2(a). The sample was comprised of crystalline ZSM-5 particles, which were dispersed on the amorphous silica–alumina matrix and exhibited characteristic diffraction contrast. The {1 0 1}-type lattice planes of zeolite ZSM-5 could be clearly identified, as shown by the HRTEM image in the inset of Fig. 2(a). The EDS point analysis also verified the difference in the Al/Si ratio between silica–alumina and the ZSM-5 zeolite. The Al/Si ratio was close to 1 for the silica–alumina particles and more than 10 times lower for ZSM-5. The presence of Co_3O_4 nanoparticles was verified by selected area diffraction (SAD) experiments, such as the one shown in the respective inset of Fig. 2(a). The main reflections of the Co_3O_4 phase were indexed in the SAD pattern and measurements of their spacing resulted in d_{220} = 0.285 nm, d_{311} = 0.244 nm, d_{422} = 0.162 nm and d_{511} = 0.157 nm, which was in full agreement with the XRD data. The majority of the metal oxide particles were evenly dispersed on silica–alumina and zeolite ZSM-5, having an average size of ~5–10 nm. However, there were several particles/crystals with larger size (up to ca. 50–60 nm in one direction), thus explaining the higher average size of ~23 nm determined by XRD. The TEM and EDS analysis of the Co(10%)/ZSM-5 catalyst after the biomass pyrolysis test verified the reduction of Co_3O_4 to metallic Co, which was observed by XRD too. This can be readily derived by both the EDS spectrum, which was acquired from the Co nanoparticles at the edge of the silica–alumina/zeolite ZSM-5 support, as well as by the SAD pattern obtained from representative Co particles in the sample. Both the SAD pattern and the EDS spectrum are shown as insets in Fig. 2(b). The reflections revealed in the SAD pattern correspond to the fcc Co phase, having a spacing of d_{111} = 0.205 nm, d_{200} = 0.177 nm and d_{311} = 0.107 nm, respectively. EDS spot-analysis at the metal particles verified that they mostly consisted of Co with the atomic oxygen ratio being less than ca. 20 at. %. The presence however of some CoO phases cannot be entirely excluded, in accordance with the very weak respective peaks that were identified in the XRD patterns of this used catalyst. Furthermore, the Co particles appeared in the form of relatively larger aggregates (~ 20–50 nm) compared to the majority of the Co_3O_4 particles in the fresh calcined catalyst.

A representative TEM image of the fresh calcined Ni(10%)/ZSM-5 catalyst is illustrated in Fig. 3. The BF TEM image in Fig. 3(a) reveals

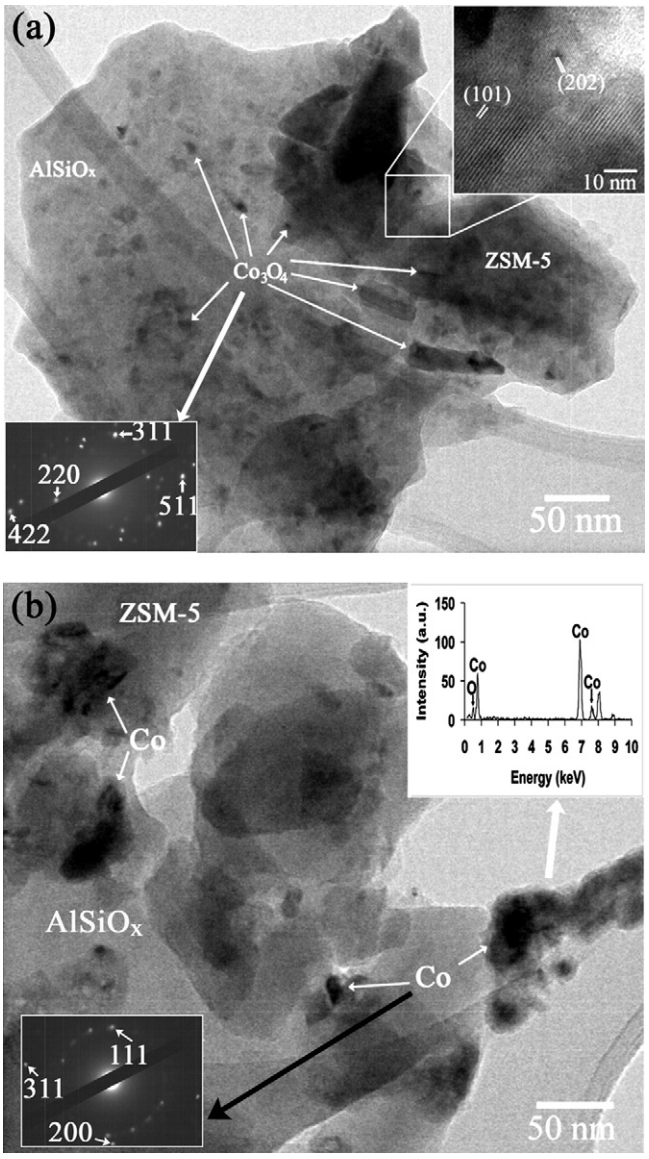

Fig. 2. TEM analysis results of the Co(10%)/ZSM-5 catalyst: (a) fresh/calcined and (b) after reaction/used. The lattice fringes in the inset HRTEM image in (a) correspond to the {1 0 1} atomic planes of ZSM-5, whereas the SAD pattern stems from the Co_3O_4 particles found on the catalyst. The main reflections of Co_3O_4 are also indexed. On the other hand, both the SAD pattern and the EDS spectrum shown as insets in (b) verify the presence of metallic cubic Co in the used catalyst.

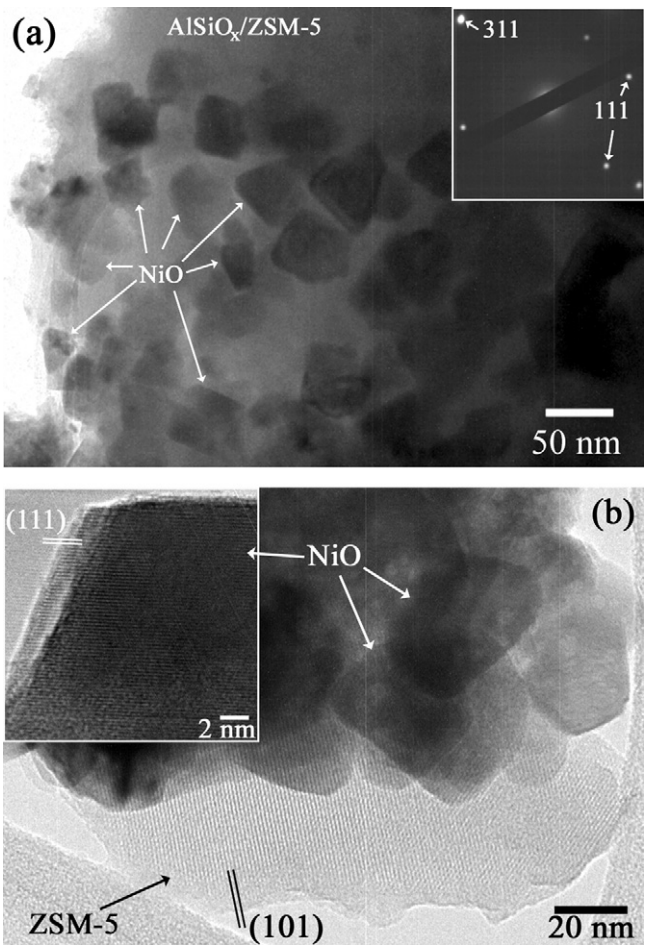

Fig. 3. (a) Conventional TEM image of the fresh/calcined Ni(10%)/ZSM-5 catalyst, revealing the morphology and dispersion of NiO particles onto the ZSM-5 zeolite and silica–alumina support. A typical SAD pattern from these NiO particles is shown in the inset. (b) HRTEM image from the same sample, revealing the crystalline structure of both the ZSM-5 zeolite and NiO phases. The zeolite and NiO particles predominately exhibit {1 0 1}- and {1 1 1}-types of lattice fringes, respectively.

that the sample comprised of characteristic rectangular or cubic NiO particles exhibiting strong diffraction contrast, which were highly dispersed on both the zeolite and the silica–alumina matrix. SAD experiments (inset in Fig. 3(a)) revealed that the particles comprised of a single crystalline NiO phase. This was also confirmed by HRTEM images of the catalyst where the characteristic {1 1 1} planes of the NiO crystals, with an average interplanar spacing of 0.243 nm, are clearly shown (inset in Fig. 3(b)). The NiO particles were larger in size compared to the Co_3O_4 ones in the Co(10%)/ZSM-5 catalyst, having a mean size of ~40–45 nm, as determined by TEM micrographs in several areas of the sample. This value was in very good agreement with the Scherrer analysis results of the XRD data (discussed above).

The BF TEM image of the Ni(10%)/ZSM-5 catalyst after the pyrolysis experiment is shown in Fig. 4. The catalyst comprised of significantly smaller (compared to the NiO ones in the fresh/calcined sample) spherical or rectangular particles, which

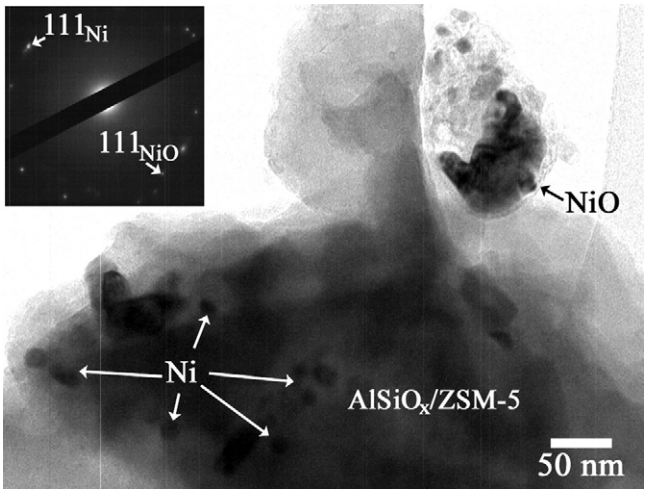

Fig. 4. Characteristic TEM image from the Ni(10%)/ZSM-5 zeolite catalyst after the pyrolysis reaction. The co-existence of metallic Ni and residual NiO particles is demonstrated both in the TEM image, as well as in the SAD pattern inset, where the {1 1 1} reflections of Ni and NiO are simultaneously observed.

Table 3
Product yields in non-catalytic flash pyrolysis of lignocellulosic biomass and in the catalytic upgrading of the biomass pyrolysis vapors.

Catalysts	Total liquid (wt.% on biomass)	Aqueous phase (wt.% on biomass)	Organic phase (wt.% on biomass)	Gases (wt.% on biomass)	Coke (wt.% on biomass)	O (org) (wt.% on organic phase)
Silica sand	58.67	21.22	37.45	18.19	23.14	40.64
ZSM-5 (pure)	34.33	28.81	5.52	31.35	31.42	4.24
ZSM-5 (diluted)[a]	48.53	27.70	20.82	25.75	25.70	30.98
CoO	56.47	22.37	34.10	21.29	22.24	34.17
Co_3O_4	55.49	26.30	29.18	33.78	22.55	35.96
Co(1%)/ZSM-5[b]	44.44	27.18	17.26	29.25	26.31	31.30
Co(5%)/ZSM-5	43.53	26.46	17.07	30.77	25.70	29.09
Co(10%)/ZSM-5	45.04	28.23	16.81	31.20	23.76	26.87
NiO	47.46	24.81	22.65	27.73	24.84	30.89
Ni(1%)/ZSM-5[b]	43.30	28.16	15.15	30.49	26.21	30.39
Ni(5%)/ZSM-5	40.09	26.51	13.59	32.27	27.03	28.74
Ni(10%)/ZSM-5	39.48	27.96	11.52	34.57	25.94	20.14

[a] Commercial equilibrium ZSM-5 catalyst diluted with silica–alumina (contains 30 wt.% crystalline zeolite).
[b] All the metal modified catalysts were prepared using the commercial ZSM-5 catalyst.

were highly dispersed on the commercial zeolite support. An average size of ~17 nm was determined by examining several TEM images, in accordance with the XRD results of this used catalyst. The particles exhibited strong diffraction contrast and SAD experiments (inset in Fig. 4) revealed that they predominately comprised of Ni in metallic form, although some remaining NiO phase was still present. The majority of the spots corresponded to the {1 1 1} lattice planes of Ni, with d_{111} = 0.2 nm; however, the presence of the 111 reflection of NiO could also be distinguished. Indeed, the TEM image in Fig. 4 shows that, except from the metallic Ni particles, some relatively big NiO crystals could also be identified with size similar to that in the fresh, calcined catalyst. The TEM experiments also revealed that, in some cases, the catalyst particles were covered by a thin layer of graphitized carbon, possibly due to the strong dehydrogenation (related to the formation of coke) function of Ni in the course of the pyrolysis process, as is discussed in more detail below. It is interesting to note that such carbon phases were not observed on the used Co(10%)/ZSM-5 catalyst.

3.2. Catalytic effects on product yields in the upgrading of biomass pyrolysis vapors

Zeolite H-ZSM-5 has been shown to be very active in catalytic biomass pyrolysis and also to enhance the selectivity towards aromatics in bio-oil [9–12,18–21,28,42,43]. The product yields in the in situ catalytic upgrading of biomass pyrolysis vapors, for the various catalysts of our study are summarized in Table 3, while the composition of the pyrolysis gases is presented in Table 4. In comparison to the non-catalytic experiments, all the catalysts decreased the total liquid yield and increased the gaseous products and coke at the expense of the organic yield. This behavior, at least for the parent H^+-forms of the zeolite catalysts, is attributed to various hydrocarbon conversion reactions, such as cracking, dehydrogenation and cyclization/aromatization, which are catalyzed by the zeolitic Brönsted acid sites [9,10,17]. In addition, water formation was enhanced in all cases due to increased dehydration/decarboxylation of the oxygenated compounds on the acid sites of zeolite ZSM-5 [24] or those on silica–alumina matrix in the commercial diluted catalyst. This latter catalytic formulation exhibited a moderate but similar behavior with that of pure crystalline ZSM-5 zeolite with respect to the changes in the product yields in biomass pyrolysis, due to its lower acidity, both in terms of number and strength of acid sites.

The catalytic performance of the pure (non-supported) CoO and Co_3O_4 metal oxides follows the same trend with that of the non-modified ZSM-5 based catalysts. However, they are less reactive in converting the organic phase of bio-oil as compared to the crystalline and the equilibrium/diluted ZSM-5 catalysts due to the mild (mainly Lewis) acidity of cobalt oxides (Tables 2 and 3). Moreover, there is a noticeable effect of Co_3O_4 on the yield of gases. The production of CO_2 was more than doubled compared to that with the non-catalytic and the ZSM-5 catalyzed experiments, while at the same time CO remains at the same level as in the non-catalytic pyrolysis. These changes in CO_2/CO yields are indicative of the different decarbonylation/decarboxylation mechanism that applies for Co_3O_4 compared to ZSM-5 due to the differences in their acidic properties (number, strength and mainly type of acid sites). Furthermore, the significantly increased production of CO_2 can be associated with the oxygen atoms that are offered by Co_3O_4 when it is reduced to CoO and metallic Co (according to the XRD and TEM results) during the pyrolysis reaction. The pure nickel oxide (NiO) is more active compared to cobalt oxides, in terms of decreasing bio-oil yield via reduction of the organic phase with consequent increase of gases and coke (slightly). This could be related with the

Table 4
Composition of gases (wt.% on biomass) produced by non-catalytic flash pyrolysis of lignocellulosic biomass and by catalytic upgrading of the biomass pyrolysis vapors.

Catalysts	H2	CO2	CO	CH4	C2H6	C2H4	C3H8	C3H6	C4–C6 alkanes
Silica sand	0.05	9.81	6.59	0.89	0.16	0.21	0.04	0.21	0.31
ZSM-5 (pure)	0.04	11.50	14.56	1.20	0.21	1.71	0.12	1.25	0.75
ZSM-5 (diluted)[a]	0.04	11.10	11.43	1.03	0.18	0.74	0.06	0.80	0.36
CoO	0.23	12.69	6.67	0.87	0.14	0.16	0.04	0.12	0.38
Co_3O4	0.50	25.92	5.75	0.96	0.13	0.12	0.04	0.09	0.27
Co(1%)/ZSM-5[b]	0.03	12.79	11.63	1.11	0.19	0.99	0.06	0.96	1.50
Co(5%)/ZSM-5	0.12	14.24	11.34	1.40	0.20	1.04	0.06	1.00	1.38
Co(10%)/ZSM-5	0.11	15.18	11.19	1.31	0.19	0.97	0.06	0.87	1.33
NiO	0.76	16.15	8.67	1.00	0.21	0.20	0.05	0.17	0.31
Ni(1%)/ZSM-5 [b]	0.10	12.54	12.97	1.50	0.22	1.03	0.06	0.87	1.20
Ni(5%)/ZSM-5	0.25	13.08	14.53	1.51	0.22	0.96	0.06	0.87	1.39
Ni(10%)/ZSM-5	0.45	15.14	14.36	1.42	0.20	0.82	0.06	0.79	1.34

[a] Commercial equilibrium ZSM-5 catalyst diluted with silica–alumina (contains 30 wt.% crystalline zeolite).
[b] All the metal modified catalysts were prepared using the commercial ZSM-5 catalyst.

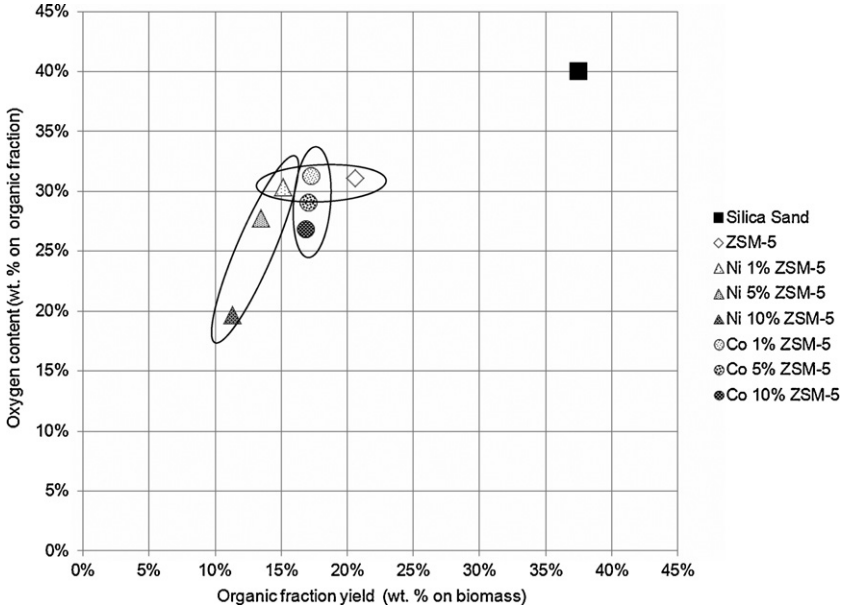

Fig. 5. Effect of the various Ni and Co-modified equilibrium ZSM-5 zeolite catalysts on the yield and oxygen content of the organic fraction of bio-oil.

slightly increased Lewis acidity of NiO compared to Co_3O_4 (derived from acidity data in Table 2). A similar effect on the yields of CO_2/CO was observed with NiO, as with Co_3O_4, but to a lesser extent.

The next step was to try and combine the above effects of the strongly acidic ZSM-5 based catalysts with those of the NiO and Co_3O_4 metal oxides, aiming at a more favorable product selectivity and bio-oil composition. The product yields obtained with the diluted ZSM-5 catalyst and the Ni or Co-modified samples are shown in Tables 3 and 4 (and in Fig. S3-Supplementary Information). The low reactivity observed for the pure Co_3O_4 oxide was confirmed also for the ZSM-5 supported catalysts. Despite the small decrease in the yield of total bio-oil (due to the small decrease of the organic phase) compared to the use of non-modified ZSM-5, it can be clearly seen from the results in Tables 3 and 4, that the increase of Co addition from 1 to 10 wt.% induces no further change in the above product yields, compared to that with the lowest Co loading of 1 wt.%. In contrast to Co_3O_4 supported catalysts, the addition of NiO in the equilibrium/diluted ZSM-5 catalyst had a systematic pronounced effect on further reducing the yield of bio-oil and its organic phase by increasing the loading of NiO in the catalyst (Table 3 and Fig. S3). This is in line with the enhanced reactivity of the pure NiO discussed above.

Some additional evidence for elucidating the reaction mechanisms can be obtained by correlating the yields of water (aqueous phase, Table 3) and of other gases; i.e. all gases except CO and CO_2 (Table 4) with those of the organic phase of bio-oil. The decrease of the organic phase with both the Ni- and Co-modified ZSM-5 catalysts does not affect the formation of water and leads mainly to increased production of H_2 and C_2–C_6 gaseous hydrocarbons, with emphasis to C_4–C_6 alkanes. Two important reaction pathways can be suggested from these results: (i) the de-oxygenation of bio-oil proceeds via decarboxylation reactions with limited formation of water and consequent saving of the in situ produced hydrogen, and (ii) the "saved" *in situ* produced hydrogen atoms could tentatively participate in hydrogen transfer reactions on the transition metals leading to increased formation of saturated hydrocarbons, via the classical carbenium ion intermediates formed on the zeolitic acid sites. The increased formation of light olefins (C_2–C_3 shown in Table 4) with the use of ZSM-5 zeolitic catalysts compared to the non-catalytic experiment and the presence of Ni and Co in reduced, metallic state in the used catalysts (verified by the XRD and TEM results) strongly support the above (ii) reaction mechanism hypothesis. On the other hand, the almost unaffected water production indicates that the oxygen of the bio-oil compounds is not removed via hydro-deoxygenation reactions that could be favored by the Ni and Co supported metals, but mostly via decarboxylation reaction pathways.

As reported in the literature [8,9], the most important problem of bio-oil, when it is considered as fuel or feedstock for high-quality fuel production, is the high concentration of oxygenates in the organic phases. Thus, reduction of oxygen content of bio-oil is one of the primary targets, which is however, in most cases, accompanied by reduced yield of liquid organic product, as can be seen for the acidic equilibrium/diluted ZSM-5 catalyst in Fig. 5, which presents the correlation between the organic fraction yield and the oxygen content of this bio-oil fraction.

The low-metal modified catalysts (with 1 wt.% metal) induced a further decrease in the organic phase of bio-oil, as compared with the performance of the unmodified ZSM-5 catalyst, without lowering the oxygen content. This effect was more pronounced with the more "reactive" supported NiO, as discussed above. However, at higher metal loadings (5 and 10 wt.%) a noticeable decrease of oxygen was observed, which in the case of Co-modified catalysts occurs with limited subsequent reduction of the organic phase. On the other hand, the enhanced decrease of oxygen with the Ni-modified catalysts was accompanied by a considerable further decrease of the organic phase. The more pronounced effect of NiO on both the yield and oxygen content of the organic fraction could be associated with its more acidic nature compared to that of supported Co_3O_4 (Table 2).

3.3. Catalytic effects on bio-oil composition

The composition of bio-oil in the non-catalytic flash pyrolysis and the biomass pyrolysis vapors upgrading experiments are shown in Figs. 6 and 7 (as well as in Table S1 – Supplementary Information). The most representative organic compounds of the thermal bio-oil are classified in 13 major functional groups: aromatic hydrocarbons, aliphatic hydrocarbons, phenols, furans, acids, esters, alcohols, ethers, aldehydes, ketones, polyaromatic hydrocarbons (PAHs), nitrogen compounds, and heavier compounds. Among them, aromatic hydrocarbons, aliphatic hydrocarbons and alcohols

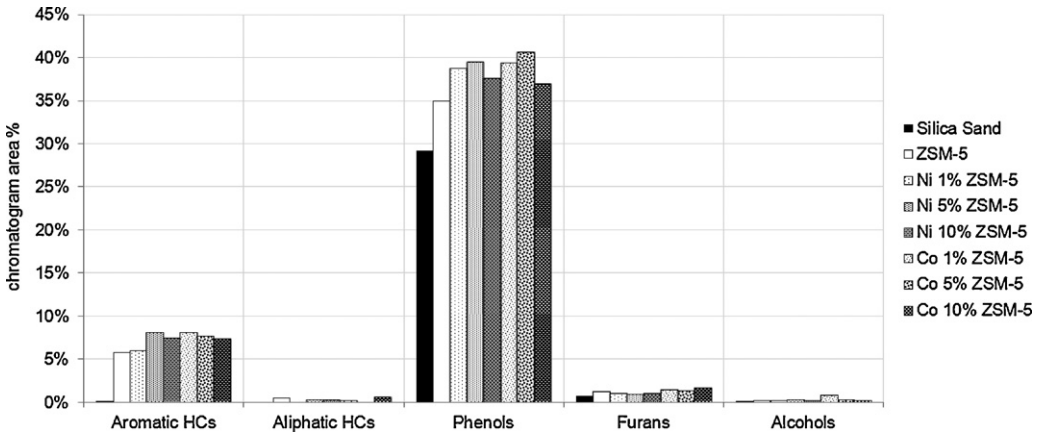

Fig. 6. Product yields of desired compounds in the organic phase of bio-oil produced by non-catalytic flash pyrolysis of lignocellulosic biomass and by catalytic upgrading of the biomass pyrolysis vapors.

are considered as desirable products for biofuels production, while phenols and furans are also regarded as high added value chemicals. On the other hand, acids are responsible for the corrosiveness of the bio-oil and thus considered undesirable. The same stands for ketones and aldehydes, which are related with the instability of the bio-oil during transport and storage. Ethers, esters and in general oxygenates are also undesirable as they reduce the heating value of the bio-oil. Finally PAHs and nitrogen compounds are detrimental for environmental reasons. The above classification in desirable (Fig. 6) and undesirable (Fig. 7) compounds has been adapted here in order to evaluate our catalytic results.

As can be seen in Fig. 6, the production of the "desirable" aliphatic hydrocarbons and alcohols, in the presence or absence of catalysts, was negligible. Furans were also slightly affected by any catalyst. On the other hand, the use of the ZSM-5 catalyst resulted in the production of some aromatics but not as high as the typical concentration values reported in the literature [9–12,18,19]. This is attributed to the dilution of crystalline ZSM-5 zeolite (30 wt.%) in a much less active silica–alumina matrix and the final equilibration (which leads to framework dealumination of crystalline zeolite and eventual decrease of its Brönsted acidity) of this catalytic formulation after subjecting to biomass pyrolysis in the pilot plant unit. When the crystalline ZSM-5 zeolite was used, a considerable increase in aromatics was observed, as can be seen in Fig. 6. The reverse behavior was observed for phenols. The very active crystalline ZSM-5 zeolite induced a small decrease of phenols compared to the non-catalytic pyrolysis oil, while the equilibrium/diluted ZSM-5 catalyst increased phenols, possibly due to the mild acidic function of the silica-alumina matrix in combination with its mesoporous nature.

Addition of the transition metals in the equilibrium/diluted ZSM-5 catalyst induced a further small increase in the relative abundance of aromatics and phenols, irrespective of the level of metal loading, for both metals (Fig. 6). The increase of aromatics could be attributed to a possible enhanced dehydrogenation pathway on the transition metals (in the overall aromatization reaction mechanism on the acid sites of ZSM-5 via oligomerization and cyclization of light, i.e. C_2–C_3, alkenes), while the increase of phenols could be related with the decrease of Brönsted sites which are masked by the metal ions (Table 2).

The above discussed reduction of Ni and Co oxides during biomass pyrolysis has not been previously reported in the literature and it is quite important when considering the possibility of commercial use of these catalysts. In such case, the catalyst will be continuously re-circulated between the pyrolysis reactor (reducing conditions) and a second fluidized reactor-regenerator (oxidizing conditions) aiming to burn off char (coke deposited on the catalyst and possibly unreacted biomass). The in situ formation of reduced metal phases (of lower oxidation state) during the pyrolysis can actually induce hydrogen transfer reactions on metallic Ni and Co (especially Ni) by using the small amounts of in situ produced H_2 or even more realistic, in a hydro-pyrolysis process where external hydrogen is fed to the reactor. Such reactions can include hydro-deoxygenation, as well as hydrogenation/saturation of

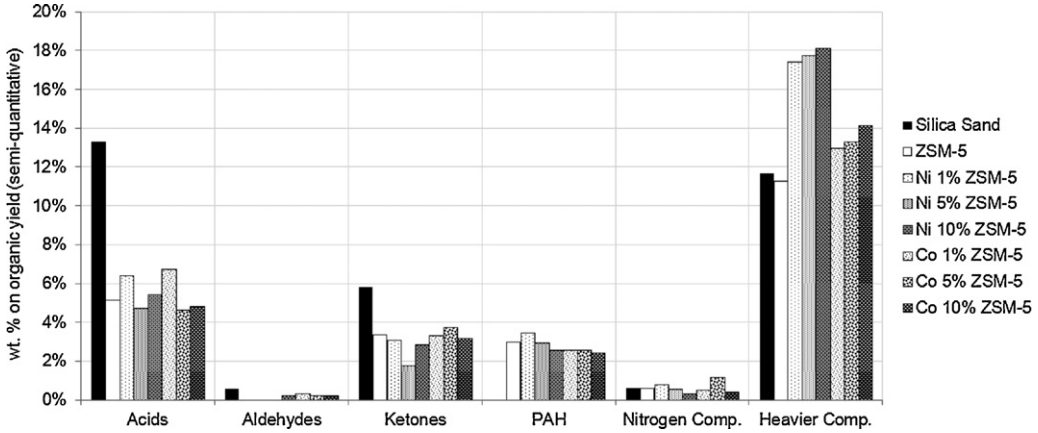

Fig. 7. Product yields of undesired compounds in the organic phase of bio-oil produced by non-catalytic flash pyrolysis of lignocellulosic biomass and by catalytic upgrading of the biomass pyrolysis vapors.

double bonds (resulting in an increased formation of alkanes). On the other hand, the combined function of metallic Ni (or Co) with the acid sites (available on the ZSM-5 support material) can provide the ideal environment for oligomerization of small alkenes followed by cyclization and dehydrogenation, leading to enhanced formation of aromatics.

With regard to the "undesirable" compounds, the carboxylic acids were reduced with the use of all catalysts compared to the non-catalytic pyrolysis, with no significant improvement by the addition of metals in the ZSM-5 catalyst (Fig. 7). Ketones were also decreased with all the catalysts. On the other hand, PAHs were produced with all the catalysts, in contrast to the non-catalytic pyrolysis oil, which does not contain any polyaromatic compounds. Aldehydes and nitrogen compounds remain negligible with all catalysts, as in the non-catalytic pyrolysis experiments. Finally modification of ZSM-5 with metal oxides, and especially NiO, resulted in enhanced selectivity towards heavier compounds.

4. Conclusions

Biomass catalytic pyrolysis is an emerging technology for the production of bio-oil suitable for use as feedstock (biocrude) in existing oil refinery processes towards high quality transportation fuels and/or for obtaining valuable chemicals. The main target in catalytic pyrolysis is to in situ produce bio-oil with less oxygen content in the organic phase as compared with the conventional bio-oil produced via thermal pyrolysis of biomass. Incorporation of transition metals (Ni or Co) in a commercial diluted ZSM-5 catalyst induced relatively small but noticeable changes in the performance of the parent ZSM-5 catalyst, with respect to product yields and bio-oil composition. The most important points were the limited reactivity of the metal-modified catalyst towards water production and the small increase of aromatics and phenols, compared to the unmodified ZSM-5 catalyst. An additional interesting observation, considered very useful for potential commercial applications, was the in situ reduction of the supported metal oxides during the pyrolysis reaction. Formation of reduced metal phases during pyrolysis was verified in the present study by detailed XRD and HRTEM analysis of the used catalysts and can actually favor hydrogen transfer reactions on metallic Ni and Co (especially Ni) by using the in situ produced or externally provided hydrogen leading to enhanced hydrogenation reactions towards light alkanes. In addition, the metallic Ni species can promote dehydrogenation reactions that favor the production of aromatics on the acid sites of zeolite ZSM-5.

Acknowledgements

This work was financially supported by the ACENET COMMON INITIATIVE HECABIO: "Heterogeneous Catalysis for the Conversion of Solid Biomass into Renewable Fuels and Chemicals" Project ACE.07.026.

Appendix A. Supplementary data

Supplementary data associated with this article can be found, in the online version, at http://dx.doi.org/10.1016/j.apcatb.2012.08.030.

References

[1] H.B. Goyal, D. Seal, R.C. Saxena, Renewable and Sustainable Energy Reviews 12 (2008) 504–517.
[2] Y.C. Lin, G.W. Huber, Energy and Environmental Science 2 (2009) 68–80.
[3] G.W. Huber, S. Iborra, A. Corma, Chemical Reviews 106 (2006) 4044–4098.
[4] R. Saxena, D. Adhikari, H. Goyal, Renewable and Sustainable Energy Reviews 13 (2009) 167–178.
[5] A. Demirbas, Energy and Conversion Management 49 (2008) 2106–2116.
[6] P.A. Della Rocca, E.G. Cerrella, P.R. Bonelli, A.L. Cukierman, Biomass and Bioenergy 16 (1999) 79–88.
[7] W.M. Lewandowski, E. Radziemska, M. Ryms, P. Ostrowski, Ecological Chemistry and Engineering S 18 (2011) 39–47.
[8] M. Stöcker, Angewandte Chemie International Edition 47 (2008) 9200–9211.
[9] H.J. Park, J.K. Jeon, D.J. Suh, Y.W. Suh, H.S. Heo, Y.K. Park, Catalysis Survey from Asia 15 (2011) 161–180.
[10] P.M. Mortensen, J.D. Grunwaldt, P.A. Jensen, K.G. Knudsen, A.D. Jensen, Applied Catalysis A: General 407 (2011) 1–19.
[11] D.J. Mihalcik, C.A. Mullen, A.A. Boateng, Journal of Analytical and Applied Pyrolysis 92 (2011) 224–232.
[12] E. Taarning, C.M. Osmundsen, X. Yang, B. Voss, S.I. Andersen, C.H. Christensen, Energy and Environmental Science 4 (2011) 793–804.
[13] M.H. Nilsen, E. Antonakou, A. Bouzga, A. Lappas, K. Mathisen, M. Stöcker, Microporous Mesoporous Materials 105 (2007) 189–203.
[14] E.F. Iliopoulou, E.V. Antonakou, S.A. Karakoulia, A.A. Lappas, I.A. Vasalos, K.S. Triantafyllidis, Chemical Engineering Journal 134 (2007) 51–57.
[15] K.S. Triantafyllidis, E.F. Iliopoulou, E.V. Antonakou, A.A. Lappas, H. Wang, T.J. Pinnavaia, Microporous Mesoporous Materials 99 (2007) 132–139.
[16] S.D. Stefanidis, K.G. Kalogiannis, E.F. Iliopoulou, A.A. Lappas, P.A. Pilavachi, Bioresource Technology 102 (2011) 8261–8267.
[17] A. Corma, G.W. Huber, L. Sauvanaud, P. O'Connor, Journal of Catalysis 247 (2007) 307–327.
[18] A. Aho, N. Kumar, A.V. Lashkul, K. Eränen, M. Ziolek, P. Decyk, T. Salmi, B. Holmbomb, M. Hupa, D.Y. Murzin, Fuel 89 (2010) 1992–2000.
[19] S. Vitolo, B. Bresci, M. Seggiani, M. Gallo, Fuel 80 (2001) 17–26.
[20] U.V. Mentzel, M.S. Holm, Applied Catalysis A 396 (2011) 59–67.
[21] Y.-T. Cheng, G.W. Huber, ACS Catalysis 1 (2011) 611–628.
[22] P.A. Horne, P.T. Williams, Renewable Energy 5 (1994) 810–812.
[23] P. Williams, P. Horne, Journal of Analytical and Applied Pyrolysis 31 (1995) 15–37.
[24] A.A. Lappas, S. Bezergianni, I.A. Vasalos, Catalysis Today 145 (2009) 55–62.
[25] J. Huang, W. Long, P.K. Agrawal, C.W. Jones, Journal of Physical Chemistry C 113 (2009) 16702–16710.
[26] R. French, S. Czernik, Fuel Processing Technology 91 (2010) 25–32.
[27] H.J. Park, J.I. Dong, J.K. Jeon, K.S. Yoo, J.H. Yim, J.M. Sohn, Y.K. Park, Journal of Industrial and Engineering Chemistry 13 (2007) 182–189.
[28] Y.-T. Cheng, J. Jae, J. Shi, W. Fan, G.W. Huber, Angewandte Chemie International Edition 51 (2012) 1387–1390.
[29] B. Valle, A.G. Gayubo, A.T. Aguayo, M. Olazar, J. Bilbao, Energy and Fuels 24 (2010) 2060–2070.
[30] G.T. Neumann, J.C. Hicks, Topics in Catalysis 55 (2012) 196–208.
[31] E. Antonakou, A. Lappas, M.H. Nilsen, A. Bouzga, M. Stöcker, Fuel 85 (2006) 2202.
[32] J. Chattopadhyay, J.E. Son, D. Pak Korean, Journal of Chemical Engineering 28 (8) (2011) 1677–1683.
[33] E. Butler, G. Devlin, D. Meier, K. McDonnell, Renewable and Sustainable Energy Reviews 15 (2011) 4171–4186.
[34] A.G. Gayubo, B. Valle, A.T. Aguayo, M. Olazar, J. Bilbao, Journal of Chemical Technology and Biotechnology 85 (2010) 132–144.
[35] A.A. Lappas, V.S. Dimitropoulos, E.V. Antonakou, S.S. Voutetakis, I.A. Vasalos, Industrial and Engineering Chemistry Research 47 (2008) 742–747.
[36] C.A. Emeis, Journal of Catalysis 141 (1993) 347–354.
[37] http://www.iza-structure.org/databases
[38] C.S. Triantafillidis, A.G. Vlessidis, L. Nalbandian, N.P. Evmiridis, Microporous and Mesoporous Materials 47 (2001) 369–388.
[39] V.G. Komvokis, S.A. Karakoulia, E.F. Iliopoulou, M.C. Papapetrou, I.A. Vasalos, A.A. Lappas, K.S. Triantafyllidis, Catalysis Today, in press.
[40] N.Y. Topsoe, K. Pedersen, E.G. Derouane, Journal of Catalysis 70 (1981) 41.
[41] G.I. Kapustin, T.R. Brueva, A.L. Klyachko, S. Beran, B. Wichterlova, Applied Catalysis 42 (1988) 239–246.
[42] S. Stephanidis, C. Nitsos, K. Kalogiannis, E.F. Iliopoulou, A.A. Lappas, K.S. Triantafyllidis, Catalysis Today 167 (2011) 37–45.
[43] R. Torren, Z. Carlson, A. Geoffrey, Z. Tompsett, C. William, Z. Conner, W.G. Huber, Topics in Catalysis 52 (2009) 241–252.